electronics

MDPI

Article

Highly Sensitive Sensor Structure Based on Sol-Gel Waveguide Films and Grating Couplers

Paweł Karasiński [1,*], Andrzej Kaźmierczak [2], Magdalena Zięba [1], Cuma Tyszkiewicz [1], Katarzyna Wojtasik [1] and Paweł Kielan [3]

[1] Department of Optoelectronics, Silesian University of Technology, B. Krzywoustego 2, 44-100 Gliwice, Poland; magdalena.zieba@polsl.pl (M.Z.); cuma.tyszkiewicz@polsl.pl (C.T.); katarzyna.wojtasik@polsl.pl (K.W.)
[2] Institute of Microelectronics and Optoelectronics, Warsaw University of Technology, Koszykowa 75, 00-662 Warszawa, Poland; andrzej.kazmierczak@pw.edu.pl
[3] Department of Mechatronics, Silesian University of Technology, Akademicka 10A, 44-100 Gliwice, Poland; pawel.kielan@polsl.pl
* Correspondence: pawel.karasinski@polsl.pl

Abstract: The technologies of optical planar evanescent wave chemical and biochemical sensors require chemically resistant, high refractive index waveguide films having very good optical transmission properties. In this paper we present such two-compound SiO_x:TiO_y waveguide films fabricated by using the sol-gel method and the dip-coating technique. These films not only have high optical quality and low propagation losses but also an extremely high refractive index of >1.90 (λ = 632.8 nm). Further we demonstrate efficient and simple sensing structures, designed and fabricated based on these films. For this purpose, grating couplers with a period of Λ = 417 nm were fabricated on the interface between a waveguide film and cover using the single-step nanoimprint method. These sensing structures were tested as planar refractometers. The results of the theoretical analysis on the basis of which the structures were designed as well as results of their experimental characterization are presented in this work. Consequently, the relationship between parameters and the sensitivity of investigated sensing structures is discussed. As a result, the profitable properties of the designed grating coupler sensors are verified and excellent consistency between the results of the theoretical analysis and experimental results is achieved.

Keywords: optical planar sensor; planar waveguide; integrated optics; grating coupler; sol-gel; refractometer

Citation: Karasiński, P.; Kaźmierczak, A.; Zięba, M.; Tyszkiewicz, C.; Wojtasik, K.; Kielan, P. Highly Sensitive Sensor Structure Based on Sol-Gel Waveguide Films and Grating Couplers. *Electronics* **2021**, *10*, 1389. https://doi.org/10.3390/electronics10121389

Academic Editor: Esteban Tlelo-Cuautle

Received: 31 March 2021
Accepted: 7 June 2021
Published: 9 June 2021

1. Introduction

Integrated optics applications have been developed since the late 1960s [1,2]. Currently, the application areas are predominantly focused on telecommunication and sensory systems. In both cases one deals with optical systems integrated on a single planar substrate, which are based on the same set of subcomponents and operate on the same physical principles. Grating couplers are among the fundamental integrated optics subcomponents for both these application areas. They are used for vertical light coupling to an integrated optical system from an external light source directly or via an optical fiber [3–7]. The sensing structure presented in this work takes advantage of the properties of grating couplers.

Currently, the integrated optics for telecommunication applications is being developed for the NIR spectral range, which is predominantly based on two material platforms, namely: silicon-on-insulator (SOI) and indium phosphide (InP) [8–10]. The material platform based on silicon nitride (Si_3N_4) is a complement to the above mentioned in the VIS-NIR spectral range [5,11]. Moreover, the application of polymeric materials in the integrated optics has attracted considerable attention in recent times [12–14]. With regard to sensory applications, and in particular to integrated optics planar evanescent wave sensors that are widely used in chemical and biochemical measurements, those systems

are mainly designed for the VIS spectral range. Waveguide films for these applications should have not only good transmission properties, but also should be chemically resistant. Furthermore, parameters of such waveguide films should be stable over longtime periods [15]. Compounds that are the most resistant to acids, bases and organic solvents are transition metal oxides such as: TiO_2, ZnO, ZrO_2, HfO_2. Thanks to the wide optical band gap, those materials offer good transmission properties in the Vis-NIR spectral range. Many research groups, using different technologies, have carried out research on fabrication of planar waveguides based on these materials. There are many articles presenting fabrication methods and discussing optical properties of waveguide films made of transition metal oxides. Their authors almost always conclude that these films can be applied as waveguides pointing only on a value of their refractive index. Some authors support this claim using the m-line spectroscopy technique to demonstrate the excitation of guiding modes. However, only few authors present the results of measurements of optical losses and in that case presented waveguide films have either refractive index slightly greater than substrate [16,17] or are thick enough to support multimode propagation [18]. Until now, few results of optical loss measurements in single-mode waveguide films with high refractive index have been presented.

Bradley et al. [19] have presented that both amorphous and polycrystalline anatase waveguide films (>2.4) can be fabricated by using a reactive sputtering method. They have reported propagation losses of about 1.2 dB/cm for amorphous films and >20 dB/cm for polycrystalline films, at a wavelength λ = 632.8 nm. Heideman et al. [20] have presented ZnO waveguides, fabricated using a RF magnetron sputtering, having refractive index in range of 1.93–1.96 (at λ = 632.8 nm). They have reported that propagation losses were in range of 1–3 dB/cm. Therefore, with the application of sputtering methods it is possible to fabricate planar waveguide films having optical losses slightly larger than 1 dB/cm. However, these methods have low production yield which makes them more appropriate for wafer-scale processes. The sol-gel fabrication method, presented in this paper, is very efficient and cost-effective when applied for fabrication of waveguide films. This method is also used by a number of research groups for fabrication of either single-component or multi-component films. In Reference [21], erbium doped ZrO_2 waveguides are presented. They have a refractive index in the range of 1.83–1.92 and optical losses exceeding 1 dB/cm. The authors of that paper have also reported that optical losses have been increasing with the annealing temperature. They have achieved the lowest optical losses of 1.2 dB/cm for the waveguide film having thickness d = 607 nm, annealed at the temperature of 300 °C. In Reference [22], Touam et al. presented the development of two-mode amorphous TiO_2 waveguide films fabricated using the sol-gel method and annealed at the temperature of 350 °C. The authors have reported achievement of optical losses of about 0.5 dB/cm for the TE_0 mode in the waveguide film having refractive index $n \sim 1.97$ and thickness d = 358 nm. The authors have also reported that TiO_2 waveguide films ($n \sim 2$, d = 336 nm) annealed at the temperature of 500 °C have been polycrystalline. The optical losses of these waveguides for the TM_0 mode have been 0.8 dB/cm. However, the careful analysis of the Figure 6 in Reference [22] shows that the optical losses can actually be higher than the reported value. The reasoning behind that supposition is backed by high values of root mean square (RMS) surface roughness of those films (Table 2 in Reference [22]). The influence of waveguide films parameters on optical attenuation coefficients have been discussed in Reference [23]. The sol-gel derived waveguide films presented in that work have been bimodal, whereas evanescent wave spectroscopy related applications require single mode waveguides. Moreover, the lowest propagation losses have been achieved as a result of the reduction of the temperature of annealing processes. However, as a result of the reducing of the annealing temperature organic residues in waveguide films, remnants of hydrolysis and condensation processes, are not completely removed. Such waveguides can be unstable over long time periods and in the case of their application in evanescent wave sensors, the organic remnants may interact with sensitive films in unpredictable ways. Elimination of organic remnants requires annealing processes carried out at temperatures exceeding 430 °C. However, generally in this case, a polycrystalline structure is formed in single-component films. There

is a method enabling fabrication of amorphous films annealed at even higher temperatures. It consist of using two-component films, e.g., combining transition metal oxides with silicon dioxide. In this paper we present two-compound SiO_x:TiO_y single mode waveguide films. Such films have been fabricated since the year 1983 [24,25]. Their refractive indices can be tailored by selection of the molar ratio of input reagents. However, it is becoming increasingly hard to obtain homogeneous compositions with increasing content of titania. It is noticeable that homogeneity is a necessary condition for obtaining low optical losses. There is a view in the literature that there is a tendency of glasses to crystalize if the molar content of titania exceeds 10% [26,27]. Other research groups have so far reported the development of low-loss SiO_x:TiO_y waveguide films with a maximum refractive index of about 1.75 [24,25,28–30]. The development of waveguide films having a refractive index of about 1.80 has been reported in our previous articles [31–33]. In this work we present SiO_x:TiO_y waveguide films with a very high refractive index, exceeding 1.90 (at λ = 632.8 nm) and demonstrating low propagation losses. Waveguide films with such a high refractive index, fabricated using the sol-gel method and dip-coating technique have not been presented in the literature so far. In this paper we also present the application of these films for the design and fabrication of sensor structures based on grating couplers. The latter have been fabricated using a nanoimprint method and have a period of 417 nm. We have tested the operation of these structures as refractometers.

The refractive index measurements are one of the fundamental types of measurements in biochemistry [34,35]. Sensor structures with input grating couplers were for the first time used for sensing applications by the research team led by Lukosz et al. [25,36]. The research group led by Szendrö and Vörös has also achieved a great deal in this research area [28–30]. Our grating couplers have been fabricated using the same method that was used by these two research groups. However our structures consists waveguide films having higher refractive index.

From the point of view of the fabrication of two-component SiO_x:TiO_y waveguide films using the sol-gel method, the crucial problem is the development of the homogeneous sol. That is because titanium is more active than silicon, as a result of which has tendency to form separate phase and to crystallization. Consequently, a roughness of waveguide film interfaces increases that leads to a substantial increase of scattering losses. Moreover, the nanocrystallites formed in the bulk are sources of additional scattering losses.

The purpose of this article is to present the result of our new investigations on planar waveguide sensing structures with grating couplers. The novelty consist in the development and application of the new material platform characterized by high refractive index contrast ($n \sim 1.92$) and low propagation losses. The sensing structures we fabricated are highly sensitive to refractive index variations of the medium they are covered with. These structures demonstrate also low threshold values for a detection of refractive index variations (resulting in low detection limit). This is a result of the use of high refractive index waveguides. Such advantageous properties makes them suitable for biomedical measurement applications.

The paper is organized as follows. Section 2 presents the theoretical basis of the grating coupler as a sensor element. It also includes results of the theoretical analysis showing the influence of waveguide film parameters on their homogeneous and surface sensitivity. As the result of the latter, the optimal values of waveguide film thickness have been determined, for which those sensitivities are maximum. Section 3 presents the technology of waveguide films and methods of their characterization. This section also contains the results of our investigations of fabricated sensing structures with grating couplers in the context of their application as refractometers, as well as discussion on the related findings of other researchers.

2. Theoretical Background

2.1. Grating Coupler

A schematic diagram of the sensor structure with a grating coupler is shown in Figure 1. The waveguide film of thickness d and refractive index n_1 is on the top of the optical substrate

of refractive index n_b. The grating coupler has a form of a periodic disturbance, with period $\mathbb{J}$I, of the waveguide film top interface. On the top of the waveguide film there is the sensitive film of thickness w_s and refractive index n_{ws}. Above the sensitive film there is the uniform medium having refractive index n_c (cover/ambient). Suppose that such a structure is illuminated with the collimated and polarized light beam of wavelength λ. Changing the angle of incidence θ, the incident light beam will be coupled to a waveguide film for a certain value θ_r, exciting a given waveguide mode. This is the resonant phenomenon.

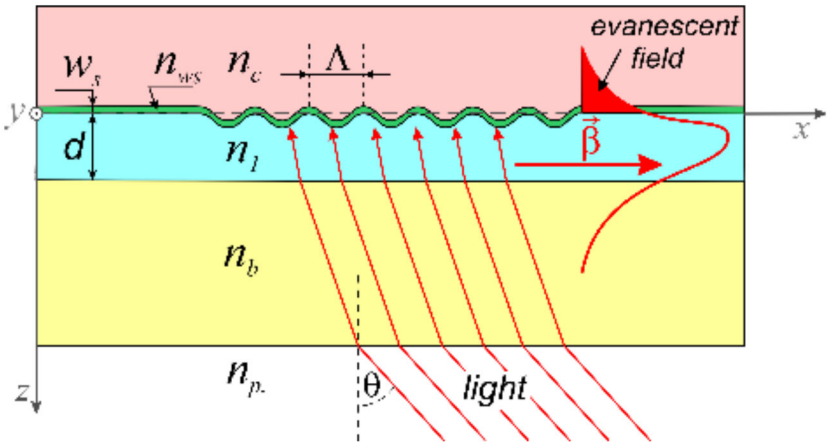

Figure 1. Planar sensor structure with a grating coupler.

The coupling angle θ_r depends on the wavelength and the polarization of the incident beam, parameters of the waveguide film (n_1, d), parameters of the sensitive film (n_{ws}, w_s), refractive indices of the substrate n_b and cover n_c. Finally it depends on the grating coupler period $\mathbb{J}$I. The operating principles of chemical/biochemical sensors rely on phenomenon that the resonant coupling angle θ_r depends on the cover refractive index n_c, thickness of the sensitive film w_s and its refractive index n_{ws}. The resonant coupling of the incident light beam to a mode of the waveguide film takes place if the phase matching condition is fulfilled:

$$\vec{\beta} = \vec{k}_{px} \pm r\vec{G} \tag{1}$$

where $\vec{\beta}$ is a propagation constant of a guided mode, $\vec{k}_{px}$ is a wave vector longitudinal component of the incident beam illuminating the grating coupler, $\vec{G}$ is a wave vector of periodic disturbance of a surface of the waveguide film and $r = \pm 1, \pm 2 \ldots$ is a diffraction order. A magnitude of the longitudinal component of the incident beam does not change with the transition into subsequent medium, therefore $k_{px} = k_{1x}$. It is a consequence of the Snell-Descartes law.

Two cases of the condition (1) i.e., $r = \pm 1$ are illustrated in Figure 2. A propagation constant of the guided mode fulfills the following condition:

$$\frac{2\pi}{\lambda_0} n_b < \beta < \frac{2\pi}{\lambda_0} n_1 \tag{2}$$

Therefore in the first case (Figure 2a, $r = +1$) the guided mode is propagating to the right, whereas in the second case (Figure 2b, $r = -1$) is propagating to the left. It is convenient to conduct the further analysis in terms of the waveguide mode effective index N that is related to the propagation constant by equation $\beta = \frac{2\pi}{\lambda} N$. Considering two additional relations: $k_{px} = \frac{2\pi}{\lambda} n_p \cdot \sin\theta_r$ and $G = 2\pi/\Lambda$, the phase matching condition takes the form of:

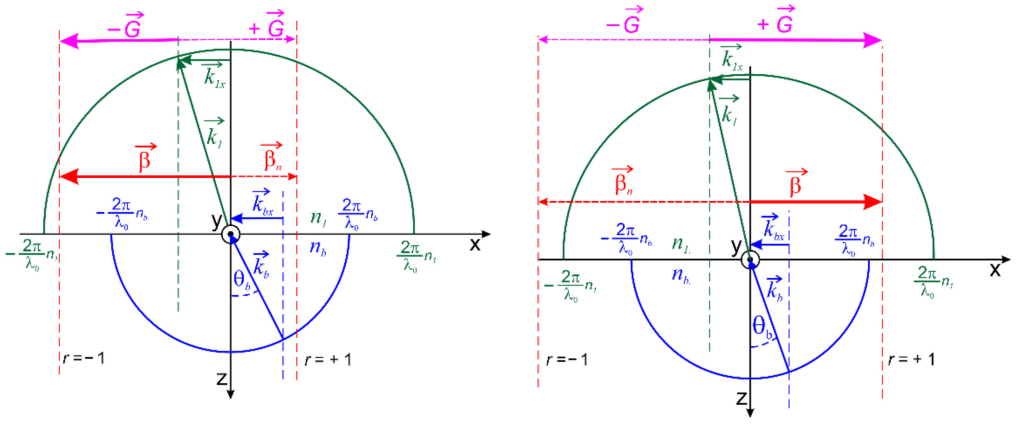

Figure 2. Wave-vector diagrams for coupling an incident light beam to a slab waveguide in the case of co-directional coupling (**a**) and counter-directional coupling (**b**) case, respectively.

$$\sin\theta_r = n_p^{-1} \cdot \left(N - r\frac{\lambda}{\Lambda}\right) \tag{3}$$

Our further considerations are carried out under the assumption that wavelength λ is constant. The Equation (3) shows the dependence of the resonant coupling angle θ_r on period $\Lambda$of the grating coupler. The relevant characteristics for the first three values of the diffraction order r are presented in Figure 3. These characteristic were calculated for a value of the effective index N = 1.52. This value is accessible for waveguide films presented in experimental part of this work.

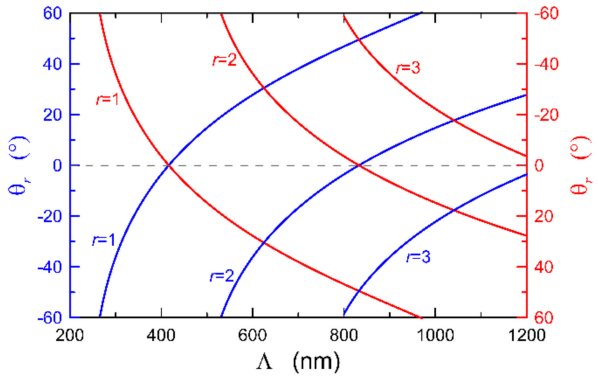

Figure 3. Dependences of coupling angle on grating coupler period for effective index N = 1.52 and wavelength λ = 632.8 nm.

One can observe on Figure 3 that the waveguide mode having effective index N = 1.52 can only be excited in the first diffraction order (r = 1) if the grating period Λ< 500 nm. Whereas for gratings having longer periods excitation is also possible for higher diffraction orders. However, a coupling efficiency is decreasing with the increase in the diffraction order r because in this case one is dealing with diffraction at higher harmonics. It is also apparent that the resonant coupling angle θ_r can assume both positive and negative values. A sense of the propagation vector $\vec{\beta}$ of the excited mode complies with the longitudinal component of the incident beam (Figure 2a) for positive values of θ_r, whereas for negative values of θ_r these vectors have opposite sense (Figure 2b). Resonant excitation of a waveguide mode for a negative coupling angle is depicted in Figure 1. In that case, excitation shall be registered by a photodetector placed at the right-hand side of the structure. Similar situation takes places if the structure is illuminated from the left-hand

side. Then, the range of negative angles is corresponding to the excitation of modes propagating to the left-hand edge of the structure. Therefore, characteristics plotted with red lines correspond to the photodetector placed at the right-hand side of the structure, whereas the blue ones correspond to a photodetector placed at its left-hand side. Both families of characteristics are symmetric with respect to line $\theta_r = 0$. This feature has practical application in measurement systems with grating couplers (Section 3.2).

2.2. Sensing Structure

The operational principle of planar evanescent wave sensors with grating couplers uses the dependence of the resonant coupling angle θ_r on the effective index N (Equation (2)). The assumption that changes of either the refractive index of the cover n_c or thickness of the sensitive film w_s are small, allows to express a change of the coupling angle in the following form:

$$\Delta\theta_r = \left(\frac{\partial\theta_r}{\partial N}\right)\left[\left(\frac{\partial N}{\partial n_c}\right)\Delta n_c + \left(\frac{\partial N}{\partial w_s}\right)\Delta w_s\right] \tag{4}$$

where [31]:

$$\frac{\partial\theta_r}{\partial N} = \left[n_p^2 - \left(N - r\frac{\lambda}{\Lambda}\right)\right] \tag{5}$$

is a sensitivity of the resonant coupling angle θ_r to changes of the effective index. The two remaining derivatives $(\partial N/\partial n_c)$ and $(\partial N/\partial w_s)$ are called homogeneous sensitivity and surface sensitivity, respectively [36].

The Equation (4) reveals that the magnitude of the change in resonant coupling angle resulting from changes in refractive index of the cover n_c or thickness of the sensitive film w_s, depends on the sensitivity of the resonant coupling angle to changes of the effective index $(\partial\theta_r/\partial N)$ and on homogeneous $(\partial N/\partial n_c)$ and surface sensitivity $(\partial N/\partial w_s)$, respectively. Characteristics demonstrating how the sensitivity $(\partial\theta_r/\partial N)$ depends on period $\Lambda$are shown in Figure 4. They are grouped in two families differing in diffraction order. Three characteristics calculated for different effective index values belong to each family. One can see that this sensitivity depends primarily on the coupler period $\Lambda$and the diffraction order r, whereas the dependence on waveguide film parameters is much less profound. The latter occurs through the effective index N and is minor within a range of small resonant coupling angles (Figures 3 and 4). Limiting considerations to the first diffraction order, one can see that sensitivity is practically independent on the effective index N for a coupler of period Λ< 400 nm, where it reaches the minimum value. For periods Λ< 400 nm this sensitivity decreases along with the increase of N, while for Λ> 400 nm it increases. For small values of the resonant coupling angle $(\partial\theta_r/\partial N)$ sensitivity values are close to unity. This indicates that the sensitivity of a structure presented in Figure 1 depends solely on parameters of the waveguide film, wavelength λ and polarization. The sensitivity can be almost doubled by selecting higher values of the grating period Λ. However in this case, the resonant coupling angle would assume values at least several dozens of angular degrees, which in practice would lead to considerable increase in duration of measurements.

Theoretical analysis of the homogeneous sensitivity was carried out for the three-layered waveguide structure. The latter is composed of a waveguide film having refractive index n_1 that is placed on the top of a substrate having refractive index n_b = 1.520. The waveguide film is covered from above by the uniform medium of refractive index n_c = 1.333 that is corresponding to water. This way, results of the theoretical analysis may be used in biochemical measurements wherein samples are very often in form of liquids having refractive indices close by value to water. Characteristic equations for the analyzed structure have the form of:

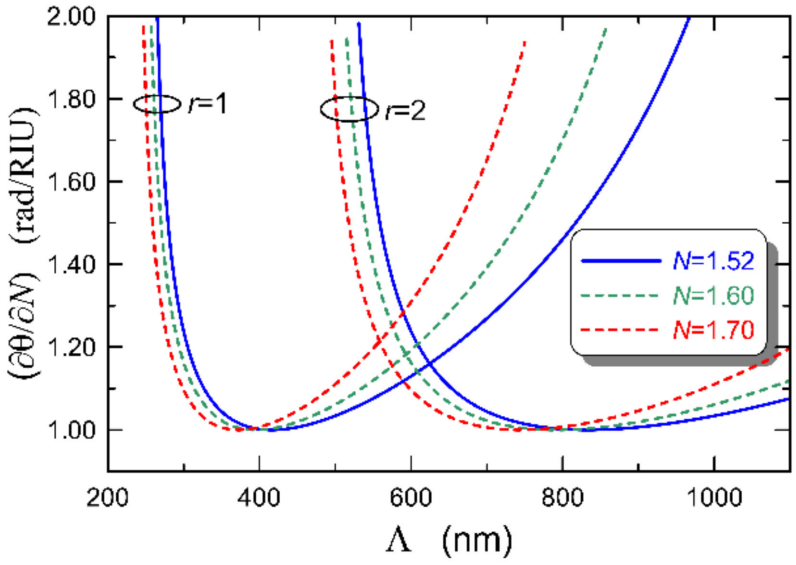

Figure 4. Calculated sensitivity of the resonance coupling angle with respect to a period of the grating coupler for three different values of the effective index and for wavelength λ = 632.8 nm.

$$\tan^{-1}\left[\left(\frac{n_1}{n_b}\right)^{\rho}\sqrt{\frac{N^2-n_b^2}{n_1^2-N^2}}\right]+\tan^{-1}\left[\left(\frac{n_1}{n_c}\right)^{\rho}\sqrt{\frac{N^2-n_c^2}{n_1^2-N^2}}\right]=\frac{2\pi}{\lambda}d\sqrt{n_1^2-N^2}+m\pi \quad (6)$$

where ρ = 0, 1 for polarization TE and TM, respectively.

In turn, theoretical analysis of the surface sensitivity require investigation of the four-layered structure. The additional layer, called sensitive, is placed on the interface of the waveguide film to the cover. This layer of thickness w_s = 1 nm and refractive index n_s = 1.5 acts as the sensitive film. Both structure types were analyzed with the application of the transfer matrix method [32]. Modal characteristics for three selected values of the waveguide film refractive index n_1 are presented in Figure 5. The range of thickness of the waveguide film is corresponding to single mode operation regime depends on the magnitude of n_1. In particular, considering the TE polarization, the following ranges have been established: d = 69 ÷ 501 nm for n_1 = 1.70, d = 65 ÷ 388 nm for n_1 = 1.80 and d = 49 ÷ 323 nm for n_1 = 1.90. In the further part of this section our considerations are limited to single mode slab waveguides. Characteristics of the homogenous $(\partial N/\partial n_c)$ and surface sensitivity $(\partial N/\partial w_s)$ with respect to a thickness of the waveguide film are presented in Figure 6. They are grouped in two families differing in polarization. Three characteristics calculated for previously selected values of n_1 belong to each family. Certain patterns are easy to observe. Both, the homogeneous and surface sensitivity reach their maxima for a thickness of the waveguide film slightly larger than a cut-off thickness for the fundamental mode of a specified polarization. Moreover, one can observe that maximum of either the homogeneous or surface sensitivity increases with increasing value of n_1. Assuming that refractive index of the waveguide film increases from 1.8 to 1.9, one can observe from the comparison of homogeneous and surface sensitivity characteristics that the maximum value of the former increases of 22% and 19% for TE_0 and TM_0 mode, respectively. Whereas, for these modes, the increase of the surface sensitivity is 30% and 26%, respectively. One can also see from the calculation results presented in Figure 6 that the optimal value of the waveguide film thickness d_{opt}, for which sensitivity is maximum, also depends on n_1. This optimal thickness decreases with increasing value of n_1. These relationships are presented in the form of charts in Figures 7 and 8. Characteristics of the maximum homogeneous and surface sensitivity with respect to a refractive index of the waveguide film are shown in Figure 7a,b, respectively. One can observe that for all values of n_1 the TM polarization is more sensitive.

The relative difference of maximum sensitivities for TM_0 and TE_0 modes is lower in case of the surface sensitivity.

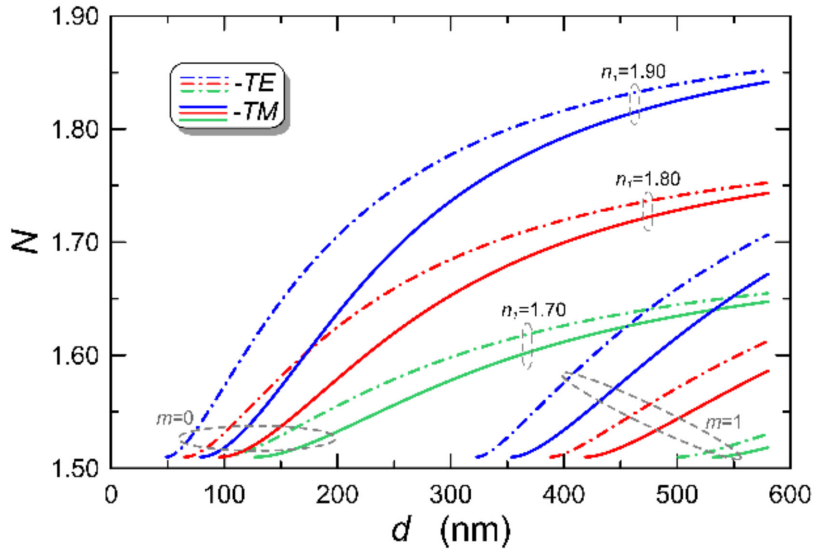

Figure 5. Modal characteristics of slab waveguides on glass substrates for selected values of the refractive index of the waveguide film. The remaining parameters have the following values: n_b = 1.510, n_c = 1.333, λ = 632.8 nm.

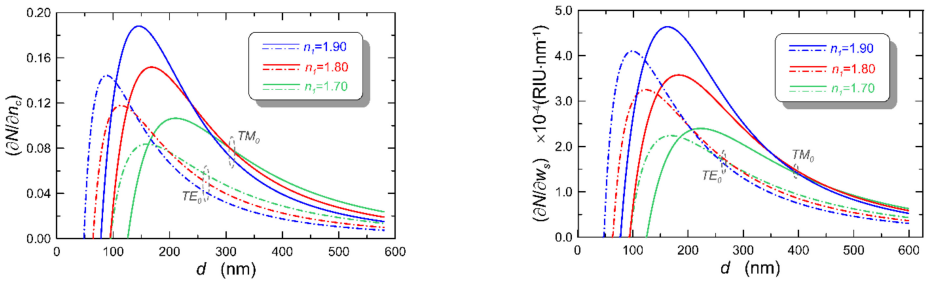

(**a**) (**b**)

Figure 6. Influence of the thickness and refractive index of waveguide films on the homogeneous (**a**) and surface (**b**) sensitivity. The remaining parameters have the following values: n_b = 1.510, n_c = 1.333, n_s = 1.500, w_s = 1.0 nm, λ = 632.8 nm.

Characteristics of the optimum thickness of the waveguide film with respect to its refractive index are presented in Figure 8. The charts show that values of d_{opt} are larger for the TM_0 mode. Regardless of the polarization, the surface sensitivity reaches its maximum for slightly larger values of d_{opt}.

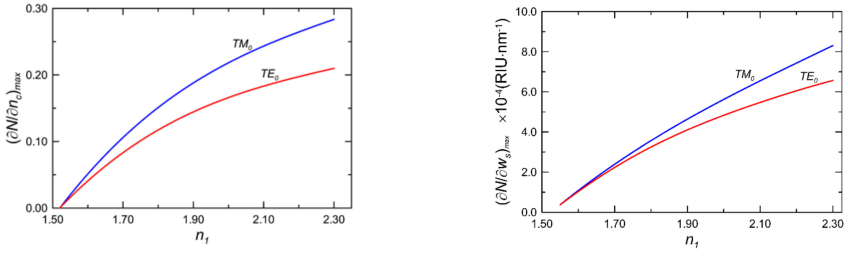

(**a**) (**b**)

Figure 7. Influence of refractive index of the waveguide film on maximum value of the homogeneous sensitivity (**a**) and surface sensitivity (**b**). Wavelength and parameters describing the planar waveguide are given in the caption of Figure 6.

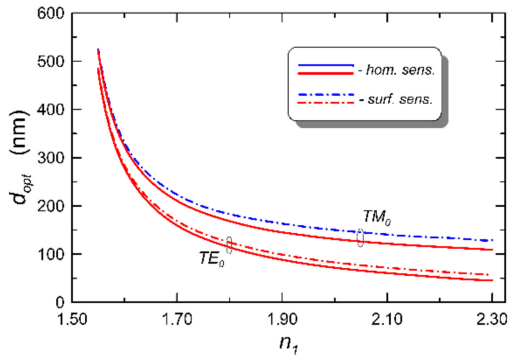

Figure 8. Optimum thickness of the waveguide films corresponding to the maximum values of the homogeneous and surface sensitivity, respectively.

3. Experimental Study

3.1. Materials and Methods

Two compound SiO_x:TiO_y waveguide films were manufactured via the sol-gel method and dip-coating technique. Tetraethoxysilane (TEOS) and titanium (IV) ethoxide (TET) were applied as precursors to SiO_x and TiO_y, respectively. These two reagents were purchased from Sigma-Aldrich. The other reagents used to synthesize sols were: deionized water, anhydrous ethanol (EtOH) and hydrochloric acid (HCl). The latter was used as a catalyst. The process of preparing the SiO_x:TiO_y sol was carried out in two stages. In the first stage, the hydrolysis of each precursor was carried out separately. Then the solutions were mixed in the appropriate proportion and the process was continued. The molar ratio TEOS:TET of sols used in the investigations was 1:1.8. The molar ratio (TEOS + TET):EtOH:H_2O was 1:7:2. For the final solutions the measured pH = 3. The final SiO_x–TiO_y synthesized sol was filtered through a 0.2 µm *PTFE syringe filter*. The produced sols were aged in tightly closed vessels at the temperature of 18 °C. The films were deposited on soda-lime microscope slide glasses (Menzel-Glaser) of the dimensions 76 × 26 × 1 mm. Glass substrates were cleaned following the procedure that involved mechanical washing in water with detergent, rinsing in deionized water, soaking in the solution of isopropyl alcohol, rinsing in deionized water, rinsing in acetone and drying. The sol from which substrates were withdrew was in the beaker shielded by a glass cylinder. The application of such a procedure helped to prevent accidental air movements, thereby improving the homogeneity of waveguide films. Films of final thicknesses varying from ~128 nm to ~198 nm were withdrawn with speeds in the range of 3.1–7.0 cm/min. Deposited films were annealed at a temperature of 500 °C for 60 min.

Sol films are liable to quick densification after deposition on substrates as a result of evaporation of solvents. Nevertheless over some period of time, directly after deposition, they are susceptible to deformation, which may come from mechanical strain. This property is used for the fabrication of the grating couplers using the nanoimprint method. The holographic grating of constant 2400 g/mm was used as a master grating. The replication of the master grating structure onto waveguide films was followed by their annealing at a temperature of 500 °C for 60 min.

The refractive index and thickness of the fabricated waveguide films were measured using monochromatic ellipsometer SENTECH SE 400 (Sentech model 2003, Berlin, Germany). Transmittance and reflectance spectra were measured over the range of 200–1100 nm using a UV–VIS AvaSpec-ULS2048LTEC spectrophotometer (Avantes) and lab-grade Reflection Probes QR400–7-SR (Ocean Optics). The deuterium-halogen lamp AvaLight-DH-S-BAL (Avantes) was used as the light source.

Finally, the refractometric properties of the sensor structures (PS) fabricated this way were investigated using the experimental setup presented in Figure 9. The influence of the cover refractive index n_c on the resonant excitation angle θ_r of waveguide modes, was determined with the use of the goniometer GO. The sensor structure was coupled

to the measuring chamber (MC) that was filled with aqueous solutions of glycerol having different refractive indices. The detection of light excitation was achieved by using photodiodes placed on both edges of a sensing structure mounted in the setup. A laser diode LD operating at wavelength λ = 676.7 nm was a source of the input light beam. Linear polarization of the latter was set and adjusted by the polarizer P and polarization rotator RP. The laser diode was controlled by alternating signal from the generator G. The goniometer was driven by a stepper motor. Electric signals from photodiodes were provided into the homodyne nanovoltmeter NH and after demodulation were registered with a data acquisition card. The setup was controlled by a PC computer.

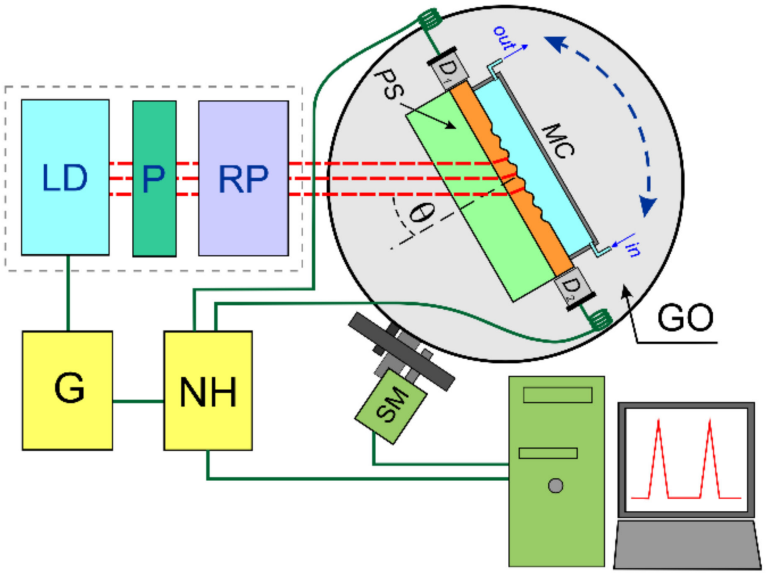

Figure 9. The schematic diagram of the measuring set-up. GO—goniometer, PS—planar sensor structure, D1, D2—photodiodes, MC—measuring chamber, LD—laser diode, P—polarizer, RP—polarization rotator, G—generator, NH—homodyne nanovoltmeter, SM—stepper motor.

3.2. Results

The dependence of the thickness and refractive index of final waveguide films on the substrate withdrawal speed are presented in Figure 10. Full square markers correspond to the experimental characteristics $d = d(v)$, whereas empty square markers correspond to the experimental characteristics $n = n(v)$. The first relationship was approximated with the second-degree polynomial by the least-squares method, whereas the second one with linear function. The thickness d increases significantly with the increase in v. Hence the latter is the main parameter by which the thickness of films fabricated using the dip-coating technique is controlled. The refractive index, in turn, increases weakly with the increase in v. The technological characteristics $d = d(v)$ and $n = n(v)$ were used in the design processes of fabrication waveguide films that have desired parameters.

It was aforementioned that homogeneous waveguide films are desired for application in evanescent wave sensors. One can relatively easily verify whether some optical layer/film is homogeneous by analyzing its reflectance spectrum. Our previous paper [33] is devoted to the issues of homogeneity of waveguide films produced by the sol-gel method. In that work, it was shown that if a given film is homogenous then interference minima on its reflectance spectrum that are far from an absorption edge lie on a reflectance spectrum of a substrate. This criterion allows us to infer about the homogeneity of the waveguide films. The exemplary reflectance spectra of silica–titania films fabricated on soda-lime substrates together with a spectrum of the substrate itself are presented in Figure 11a. As one can see, minima of reflectance spectra for wavelengths exceeding 500 nm lie on a spectrum of the soda-lime substrate, which confirms the homogeneity of those films. On the other hand, considering wavelengths below 400 nm, as the wavelength decreases the reflectance minima increasingly drift apart from the

substrate reflectance spectrum. This results from the proximity to the absorption edge that occurs at ~350 nm, as one can observe in Figure 11b. When it comes to transmission spectra, a similar regularity occurs if films are weakly absorbing. Namely, they are homogeneous if their transmission maxima far from the absorption edge lie on a transmission spectrum of the substrate. The detailed analysis of transmission spectra in the absorption region, by using the Tauc method [37,38], revealed that the absorption edge of investigated silica–titania films belongs to the spectral range of 342–351 nm. The observed shift of the absorption toward shorter wavelengths with the decrease of the film thickness is a result of the quantum size effect [39,40]. From the perspective of the accuracy of measurement, the crucial requirement is the homogeneity of the waveguide films.

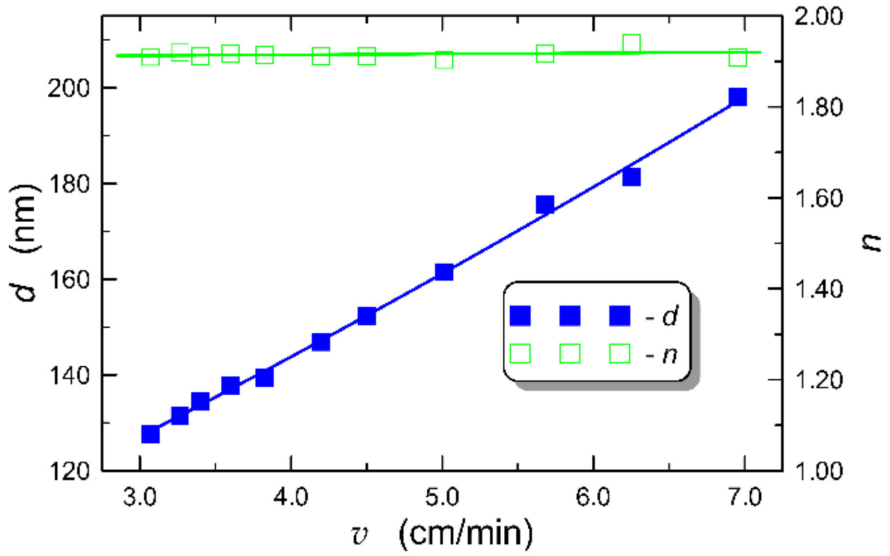

Figure 10. Experimental characteristics showing the dependence of the thickness and refractive index with respect to the substrate withdrawal speed from sol. Description of symbols: *d*—thickness, *n*—refractive index, *v*—withdrawal speed.

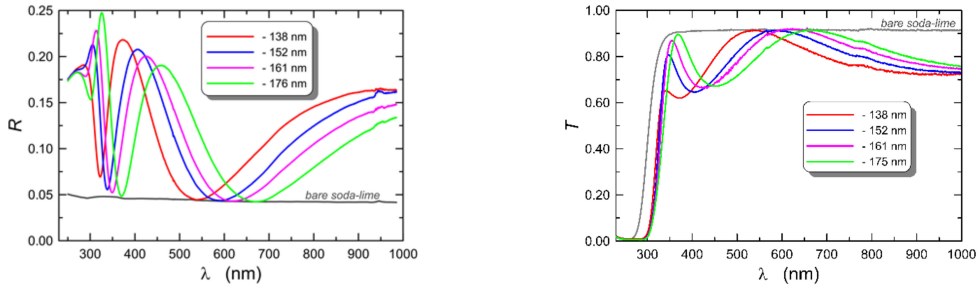

(**a**) (**b**)

Figure 11. Experimentally measured reflectance (**a**) and transmittance (**b**) spectra for selected silica–titania films on soda-lime glass substrates.

High refractive index of waveguide films is necessary to achieve high sensitivity. However, waveguide films are suitable if their transmission losses are sufficiently low. A picture presenting the slab waveguide in which the TM_0 mode was excited is shown in Figure 12. A streak of the scattered light visible on the photo has length of ~4.5 cm. The intensity of light scattered at a given point is directly proportional to light intensity reaching it. Analysis of the light intensity distribution in the streak allowed to determine that this waveguide has propagation losses at the level of ~0.3 dB/cm.

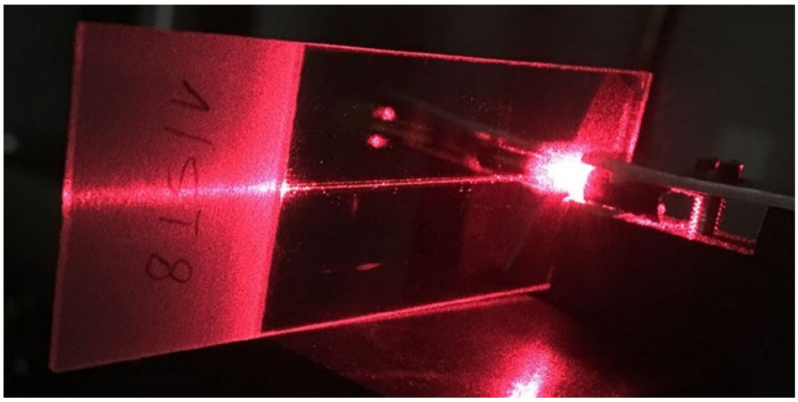

Figure 12. Image of the slab waveguide with visible streak of scattered light for excited TM_0 mode. The silica–titania waveguide film has refractive index n_1 = 1.91 and thickness d = 138 nm.

Angular characteristics of sensing structure excitations are shown in Figure 13. They were registered for different values of the cover refractive index n_c. The measurements were carried out within such range of the angle θ that each photodetector registered the in-coupling peak corresponding to excitation of a given waveguide mode (Figure 3). That way, there are two in-coupling peaks on each angular characteristic for a given value of n_c. For every angular spectrum a half of the distance between the in-coupling peaks equals the resonant coupling angle θ_r. The application of such a procedure allows to eliminate the necessity of determination the right angle direction to the top surface of the sensing structure. It should be stated that determination of the right angle direction would be a source of additional uncertainty in the process of measuring the resonant coupling angle [31]. The position of the right angle direction is plotted on Figure 13 with a dashed line. The characteristics at which in-coupling peaks are tall (signal > 2) were registered for TM polarization–the TM_0 mode was excited. The in-coupling peaks corresponding to the TE polarization are also shown. They were registered under conditions for which air was the cover layer for sensing structures (n_c = 1.0). The remaining conditions under which the measurements for both polarizations were carried out were the same. Subsequent measurements were carried out only for the TM polarization for two reasons. Namely, amplitudes of the in-coupling peaks corresponding to the TE_0 mode are low and a maximum of either the homogeneous or surface sensitivity is higher for TM modes (Figure 6). One can read from Figure 3 that for the investigated structure the resonant coupling angle is negative for each value of the cover refractive index and for each photodetector. Hence, as one can see θ_r increases with increase in n_c. The values of resonant coupling angles measured for both polarizations and for n_c = 1.0 allowed to determine the refractive index and thickness of the waveguide film. In the first step the effective indices of the fundamental modes were calculated using Equation (2). Their values are: N_{TE} = 1.6191 and N_{TM} = 1.5261. In the second step, knowing effective indices, it was possible to solve a set of two nonlinear characteristic Equation (6) for d and n_1. As a result it was determined that the thickness of the waveguide film is d = 151.3 nm and its refractive index is n_1 = 1.9102.

The characteristic presenting a dependence of the resonant coupling angle θ_r on the cover refractive index is shown in Figure 14. Square markers show the experimental dependence, whereas a continuous line represents values of the resonant coupling angle calculated on the basis of waveguide film parameters determined from the values of resonant coupling angles for n_c = 1.0. One can see excellent compatibility of calculations with the experiment.

In practice due to a dispersion of parameters characterizing technological processes, the thickness and refractive index of the waveguide film is calculated using values of θ_r measured for n_c = 1.0 and then the theoretical relationship $\theta_r = \theta_r(n_c)$ can be applied to determine a refractive index of the cover based on measured values of θ_r. The homogeneous sensitivity of the presented sensing structure is $(\partial N/\partial n_c)$ = 0.1925 for wavelength λ = 676.7 nm, whereas the surface sensitivity is $(\partial N/\partial w_s)$ = 4.31 × 10^4 (RIU · nm^{-1}).

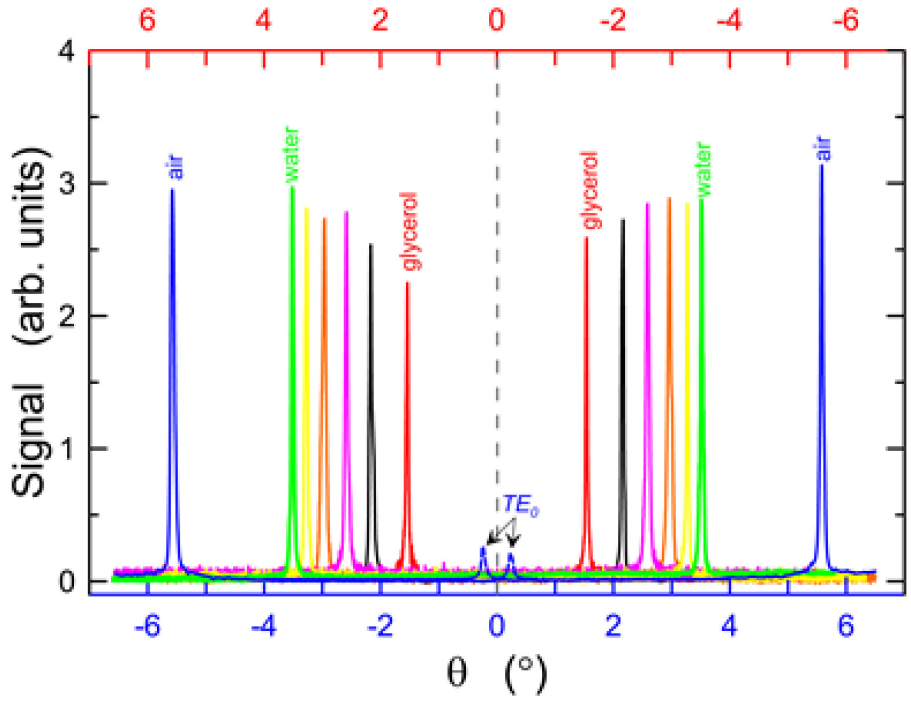

Figure 13. Modal spectra of the investigated sensing structure excited with the use of grating coupler for different refractive indices of the cover. The remaining parameters have the following values: n_b = 1.510, χ = 2400 g/mm, λ = 676.7 nm, d = 151.3 nm.

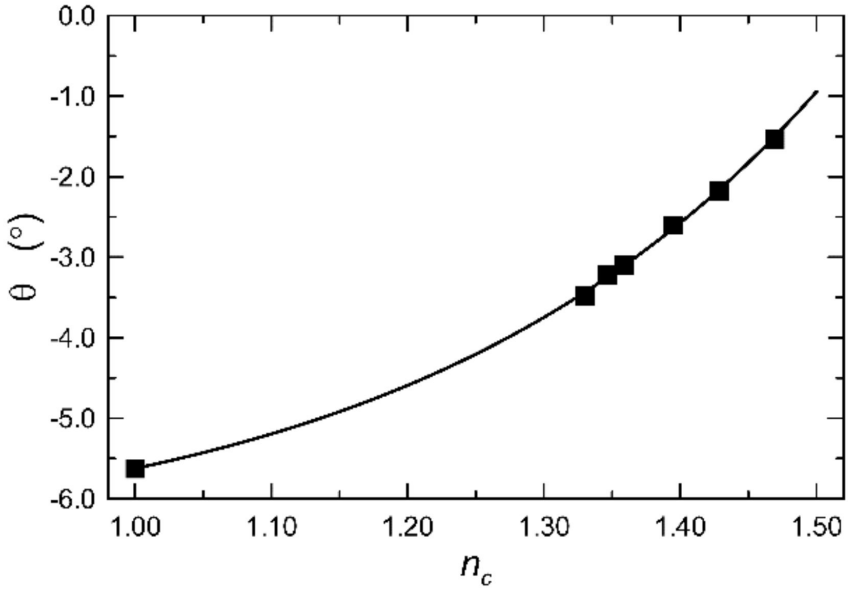

Figure 14. Experimental and theoretical characteristics of the in-coupling angles of the TM_0 mode with respect to a refractive index of the cover. The remaining parameters have the following values: χ = 2400 g/mm, λ = 676.7 nm, n_1 = 1.9102, d = 151.3 nm.

3.3. Discussion

The computational results presented in Figures 7 and 8 show that in order to achieve high homogeneous $(\partial N/\partial n_c)$ or surface sensitivity $(\partial N/\partial w_s)$ it is advisable to use waveguide films having high refractive index and carefully selected thickness. It turns out that significant technological difficulties are growing with increase in waveguide films refractive index. This is due to the fact that it is very difficult to achieve homogeneous SiO_x:TiO_y composition because

titanium is much more reactive than silicon and tends to form the separate TiO_y phase. That is why a small number of research groups have so far reported the development of technologies allowing fabrication of such films. We were able to overcome this problem and therefore waveguide films presented in this work are significantly better than those so far presented in the literature. What we have said foregoing, optical losses of our SiO_x:TiO_y waveguide films having refractive index above 1.9 are ~0.3 dB/cm. The single mode waveguide films presented in our paper have thickness of 138 nm (Figure 12). In such films the density of optical power on interfaces to the ambient and substrate is very strong. As a result the scattering on the imperfections of these interfaces is also strong. Optical losses resulting from this scattering is directly proportional to a square of the root mean square roughness characterizing these interfaces Reference [23]. Therefore, interfaces of waveguide films must be very smooth if low optical losses are to be achieved. This requirement is very difficult to meet. If waveguide films are made of polycrystalline materials then the root mean square surface roughness of their interfaces become very high. Moreover in this case additional scattering in the bulk appears. This is the reason to which exemplary amorphous waveguide films presented in cited papers of another researchers, had acceptable losses until they were underwent annealing processes. Optical losses of these films increase significantly when they are annealed at higher temperatures, because then crystallization occurs rendering them polycrystalline.

Tiefenthaler and Lukosz in Reference [41] reported SiO_2:TiO_2 waveguide films having similar refractive index, however those films have optical losses of ~2.5 dB/cm at wavelength λ = 632.8 nm. Jiwei et al. in Reference [42] presented SiO_2:TiO_2 waveguide films produced by the sol-gel method having refractive index n = 1.83 and optical loss of 7.4 dB/cm. It is instructive to compare our silica–titania waveguide films and TiO_2 films presented in Reference [22]. The latter also have optical losses equal to 0.3 dB/cm. However, we have achieved such low losses in waveguide films having their thickness optimal with respect to maximization of the homogeneous (Figure 5) and surface (Figure 6) sensitivity. The values of these sensitivities for the sensing structure presented in this work (n_1 = 1.91, d = 151 nm) are $(\partial N/\partial n_c)$ = 0.192 and $(\partial N/\partial w_s)$ = 4.31 × 10^{-4} (RIU · nm^{-1}), whereas for the waveguide film having parameters given in Reference [22] (n_1 = 1.97, d = 358 nm) one gets: $(\partial N/\partial n_c)$ = 0.0458 and $(\partial N/\partial w_s)$ = 1.72 × 10^{-4} (RIU·nm^{-1}). One can see that sensitivities of the latter are several times lower than of the sensing structure presented in this work.

The detection threshold for changes in the cover refractive index calculated for the waveguide film presented in this work (n_1 = 1.91, d = 151 nm) can be calculated from the equation below:

$$(\Delta n_c)_{\min} = \left(\frac{\partial \theta}{\partial N}\right)^{-1} \left(\frac{\partial N}{\partial n_c}\right)^{-1} (\Delta\theta)_{\min} \quad (7)$$

Its value for TM_0 mode and the cover refractive index n_c ~ 1.333 equals to $(\Delta n_c)_{\min}$ = 3.63 × 10^{-6} (RIU), whereas for waveguide films having refractive index n_1 = 1.78, reported in our former paper [31] it is $(\Delta n_c)_{\min}$ = 5.0 × 10^{-6} (RIU). One can see that application of the waveguide film whose refractive index is increased from 1.78 to 1.91 reduces the refractive index change detection threshold of 27%. The accuracy of resonant coupling angle measurements accepted for calculations results from the characteristic of our measurement setup. Its value is $(\Delta\theta)_{\min}$ = 0.7 × 10^{-6} rad [31]. The detection threshold for changes in the sensitive film thickness can be calculated from similar equation:

$$(\Delta w_s)_{\min} = \left(\frac{\partial \theta}{\partial N}\right)^{-1} \left(\frac{\partial N}{\partial w_s}\right)^{-1} (\Delta\theta)_{\min} \quad (8)$$

Assuming that average refractive index of the sensitive film is n_s = 1.5, its thickness is w_s = 1 nm and refractive index of the cover is n_c = 1.333, the value of this threshold is $(\Delta w_s)_{min}$ = 1.62 × 10^{-3} nm, whereas for waveguide films having refractive index n_1 = 1.78, the detection threshold for the change of sensitive film thickness is 2.05 × 10^{-3} nm. In this case application of the waveguide film having refractive index increased to 1.91 results

in lowering the detection threshold of 21%. The values of both detection thresholds for the sensing structures presented in this work are comparable with the values obtained by other researchers, both for sensing structures with grating couplers and other solutions [35]. The resulting values show that the sensing structure presented in this work are sufficiently sensitive for biochemical applications.

4. Conclusions

This paper presents evanescent wave sensor structure with input grating coupler. Silica–titania waveguide films having high refractive index (>1.9), optimal thickness, with respect to their homogeneous sensitivity, and low optical losses, due to their excellent homogeneity, were fabricated by using the sol-gel method and the dip-coating technique. Sensor structures were created by fabrication of grating couplers on the top of these waveguide films by using the nanoimprint method and tested by refractometric measurements.

The theoretical analysis of planar waveguide films showed that it is necessary to use films having high refractive index and optimal thickness if high sensitivity is to be achieved, either homogeneous or surface. The influence of grating coupler period on sensitivity of resonant coupling angle to changes of effective index were also discussed. It was demonstrated that both homogenous and surface sensitivity are maximum if waveguide films are single mode and their thickness is slightly larger than the cut-off thickness of fundamental TM mode. We have developed and fabricated such waveguide films. Their absorption edge occurs for wavelength lower than 350 nm. That is why these films have very good transmission properties in the Vis and NIR spectral range. For these waveguides we achieved optical transmission losses as low as ~0.3 dB/cm. Other researchers also reported such values of optical losses, but it was for films having thickness significantly larger than cut-off, being frequently bimodal for a given polarization.

Fabricated sensing structures with grating couplers were tested in the goniometer setup. The detection thresholds for changes in either the refractive index of the cover or the thickness of the sensitive film were determined. These values: $(\Delta n_c)_{min} = 3.63 \times 10^{-6}$ RIU and $(\Delta w)_{min} = 1.62 \times 10^{-3}$ nm, are lower than those for silica–titania waveguide films having refractive index $n = 1.8$. Thanks to the application of the waveguide films having a higher refractive index than before, both the minimum change detection thresholds of the ambient refractive index and sensitive film thickness can show further decreases of 27% and 21%, respectively. These parameters of the fabricated sensing structures make them suitable for biochemical measurements.

Author Contributions: Conceptualization, P.K. (Paweł Karasiński), M.Z. and C.T.; Funding Acquisition, P.K. (Paweł Karasiński), A.K. and C.T.; Investigation, P.K. (Paweł Karasiński), M.Z. and C.T.; Methodology, P.K. (Paweł Karasiński), P.K. (Paweł Kielan) and A.K.; Project Administration P.K. (Paweł Karasiński); Software, P.K. (Paweł Karasiński) and P.K. (Paweł Kielan); Supervision, P.K. (Paweł Karasiński); Validation, P.K. (Paweł Karasiński) and M.Z.; Visualization, M.Z. and K.W.; Writing—Original Draft, P.K. (Paweł Karasiński) and A.K.; Writing—Review and Editing P.K. (Paweł Karasiński), A.K. and C.T. All authors have read and agreed to the published version of the manuscript.

Funding: P.K. (Paweł Karasiński), A.K. and C.T. contributed this article within a scope of the project TANGO 3 No. 05/040/TAN19/0081 funded by National Centre for Research and Development, whereas M.Z., K.W. and P.K. (Paweł Kielan) contributed this article within a scope of the project OPUS 13 funded by National Science Centre-Poland based on the decision DEC-2017/25/B/ST7/02232.

Institutional Review Board Statement: Not applicable.

Informed Consent Statement: Not applicable.

Data Availability Statement: Not applicable.

Conflicts of Interest: The authors declare no conflict of interest.

References

1. Valette, S. Integrated optics: The history and the future. In Proceedings of the Europen Conference on Integrated Optics, Copenhagen, Denmark, 25–27 April 2007; p. WPT1.
2. Miller, S.E. Integrated Optics: An Introduction. *Bell Syst. Tech. J.* **1969**, *48*, 2059–2069. [CrossRef]
3. De Dobbelaere, P. Silicon photonics technology platform for embedded and integrated optical interconnect systems. In Proceedings of the 2013 18th Asia and South Pacific Design Automation Conference (ASP-DAC), Yokohama, Japan, 22–25 January 2013; pp. 644–647. [CrossRef]
4. Jalali, B.; Fathpour, S. Silicon Photonics. *J. Lightwave Technol.* **2006**, *24*, 4600–4615. [CrossRef]
5. Kaźmierczak, A.; Dortu, F.; Schrevens, O.; Giannone, D.; Vivien, L.; Marris-Morini, D.; Bouville, D.; Cassan, E.; Gylfason, K.B.; Sohlström, H.; et al. Light coupling and distribution for Si_3N_4/SiO_2 integrated multichannel single-mode sensing system. *Opt. Eng.* **2009**, *48*, 014401. [CrossRef]
6. Cheng, L.; Mao, S.; Li, Z.; Han, Y.; Fu, H.Y. Grating Couplers on Silicon Photonics: Design Principles, Emerging Trends and Practical Issues. *Micromachines* **2020**, *11*, 666. [CrossRef] [PubMed]
7. Ranacher, C.; Consani, C.; Hedenig, U.; Grille, T.; Lavchiev, V.; Jakoby, B. A photonic silicon waveguide gas sensor using evanescent-wave absorption. In Proceedings of the 2016 IEEE Sensors, Orlando, FL, USA, 30 October–3 November 2016; pp. 1–3. [CrossRef]
8. Arakawa, Y.; Nakamura, T.; Urino, Y.; Fujita, T. Silicon photonics for next generation system integration platform. *IEEE Commun. Mag.* **2013**, *51*, 72–77. [CrossRef]
9. Doerr, C.R. Integrated Photonic Platforms for Telecommunications: InP and Si. *IEICE Trans. Electron.* **2013**, *E96.C*, 950–957. [CrossRef]
10. Smit, M.; Leijtens, X.; Ambrosius, H.; Bente, E.; Van Der Tol, J.; Smalbrugge, B.; De Vries, T.; Geluk, E.-J.; Bolk, J.; Van Veldhoven, R.; et al. An introduction to InP-based generic integration technology. *Semicond. Sci. Technol.* **2014**, *29*, 083001. [CrossRef]
11. Wörhoff, K.; Heideman, R.G.; Leinse, A.; Hoekman, M. TriPleX: A versatile dielectric photonic platform. *Adv. Opt. Technol.* **2015**, *4*, 189–207. [CrossRef]
12. Ma, H.; Jen, A.K.-Y.; Dalton, L.R. Polymer-Based Optical Waveguides: Materials, Processing, and Devices. *Adv. Mater.* **2002**, *14*, 1339–1365. [CrossRef]
13. Bettotti, P. Hybrid Materials for Integrated Photonics. *Adv. Opt.* **2014**, *2014*, 891395. [CrossRef]
14. Zhang, Z.; De Felipe, D.; Katopodis, V.; Groumas, P.; Kouloumentas, C.; Avramopoulos, H.; Dupuy, J.-Y.; Konczykowska, A.; DeDe, A.; Beretta, A.; et al. Hybrid Photonic Integration on a Polymer Platform. *Photonics* **2015**, *2*, 1005–1026. [CrossRef]
15. Ramsden, J.J. Review of new experimental techniques for investigating random sequential adsorption. *J. Stat. Phys.* **1993**, *73*, 853–877. [CrossRef]
16. Royon, M.; Jamon, D.; Blanchet, T.; Royer, F.; Vocanson, F.; Marin, E.; Morana, A.; Boukenter, A.; Ouerdane, Y.; Jourlin, Y.; et al. Sol–Gel Waveguide-Based Sensor for Structural Health Monitoring on Large Surfaces in Aerospace Domain. *Aerospace* **2021**, *8*, 109. [CrossRef]
17. Brusatin, G.; Guglielmi, M.; Innocenzi, P.; Martucci, A.; Battaglin, G.; Pelli, S.; Righini, G. Microstructural and optical properties of sol-gel silica-titania waveguides. *J. Non Cryst. Solids* **1997**, *220*, 202–209. [CrossRef]
18. Ferrari, J.L.; Lima, K.d.O.; Gonçalves, R.R. Refractive Indexes and Spectroscopic Properties to Design Er^{3+}-Doped SiO_2–Ta_2O_5 Films as Multifunctional Planar Waveguide Platforms for Optical Sensors and Amplifiers. *ACS Omega* **2021**, *6*, 8784–8796. [CrossRef] [PubMed]
19. Bradley, J.D.B.; Evans, C.C.; Choy, J.T.; Reshef, O.; Deotare, P.B.; Parsy, F.; Phillips, K.C.; Lončar, M.; Mazur, E. Submicrometer-wide amorphous and polycrystalline anatase TiO_2 waveguides for microphotonic devices. *Opt. Express* **2012**, *20*, 23821–23831. [CrossRef]
20. Heideman, R.; Lambeck, P.; Gardeniers, J. High quality ZnO layers with adjustable refractive indices for integrated optics applications. *Opt. Mater.* **1995**, *4*, 741–755. [CrossRef]
21. Urlacher, C.; De Lucas, C.M.; Bernstein, E.; Jacquier, B.; Mugnier, J. Study of erbium doped ZrO_2 waveguides elaborated by a sol–gel process. *Opt. Mater.* **1999**, *12*, 19–25. [CrossRef]
22. Touam, T.; Znaidi, L.; Vrel, D.; Ninova-Kuznetsova, I.; Brinza, O.; Fischer, A.; Boudrioua, A. Low Loss Sol-Gel TiO_2 Thin Films for Waveguiding Applications. *Coatings* **2013**, *3*, 49–58. [CrossRef]
23. Payne, F.P.; Lacey, J.P.R. A theoretical analysis of scattering loss from planar optical waveguides. *Opt. Quantum Electron.* **1994**, *26*, 977–986. [CrossRef]
24. Herrmann, P.; Wildmann, D. Fabrication of planar dielectric waveguides with high optical damage threshold. *IEEE J. Quantum Electron.* **1983**, *19*, 1735–1738. [CrossRef]
25. Lukosz, W.; Tiefenthaler, K. Embossing technique for fabricating integrated optical components in hard inorganic waveguiding materials. *Opt. Lett.* **1983**, *8*, 537–539. [CrossRef]
26. Scannell, G.; Koike, A.; Huang, L. Structure and thermo-mechanical response of TiO_2-SiO_2 glasses to temperature. *J. Non Cryst. Solids* **2016**, *447*, 238–247. [CrossRef]
27. Kamiya, K.; Sakka, S. Thermal expansion of TiO_2-SiO_2 and TiO_2-GeO_2 glasses. *J. Non Cryst. Solids* **1982**, *52*, 357–363. [CrossRef]

28. Szendro, I. Art and practice to emboss gratings into sol-gel waveguides. In *Functional Integration of Opto-Electro-Mechanical Devices and Systems, Proceedings of the Symposium on Integrated Optics, San Jose, CA, USA, 15 May 2001*; SPIE: Bellingham, WA, USA, 2001; Volume 4284, pp. 80–87. [CrossRef]
29. Vörös, J.; Ramsden, J.; Csúcs, G.; Szendrő, I.; De Paul, S.; Textor, M.; Spencer, N. Optical grating coupler biosensors. *Biomaterials* **2002**, *23*, 3699–3710. [CrossRef]
30. Adányi, N.; Majer-Baranyi, K.; Nagy, A.; Németh, G.; Szendrő, I.; Székács, A. Optical waveguide lightmode spectroscopy immunosensor for detection of carp vitellogenin. *Sens. Actuators B Chem.* **2013**, *176*, 932–939. [CrossRef]
31. Karasiński, P. Embossable grating couplers for planar evanescent wave sensors. *Opto Electron. Rev.* **2011**, *19*, 10–21. [CrossRef]
32. Karasiński, P. Sensor properties of planar waveguide structures with grating couplers. *Opto Electron. Rev.* **2007**, *15*, 168–178. [CrossRef]
33. Karasiński, P.; Domanowska, A.; Gondek, E.; Sikora, A.; Tyszkiewicz, C.; Skolik, M. Homogeneity of sol-gel derived silica-titania waveguide films—Spectroscopic and AFM studies. *Opt. Laser Technol.* **2020**, *121*, 105840. [CrossRef]
34. Chen, Y.; Liu, J.; Yang, Z.; Wilkinson, J.S.; Zhou, X. Optical biosensors based on refractometric sensing schemes: A review. *Biosens. Bioelectron.* **2019**, *144*, 111693. [CrossRef]
35. Kozma, P.; Kehl, F.; Ehrentreich-Förster, E.; Stamm, C.; Bier, F.F. Integrated planar optical waveguide interferometer biosensors: A comparative review. *Biosens. Bioelectron.* **2014**, *58*, 287–307. [CrossRef]
36. Tiefenthaler, K.; Lukosz, W. Sensitivity of grating couplers as integrated-optical chemical sensors. *J. Opt. Soc. Am. B* **1989**, *6*, 209–220. [CrossRef]
37. Tauc, J. *Amorphous and Liquid Semiconductors*; Plenum Press: London, UK; New York, NY, USA, 1974. [CrossRef]
38. Makuła, P.; Pacia, M.; Macyk, W. How to Correctly Determine the Band Gap Energy of Modified Semiconductor Photocatalysts Based on UV–Vis Spectra. *J. Phys. Chem. Lett.* **2018**, *9*, 6814–6817. [CrossRef]
39. Kayanuma, Y. Quantum-size effects of interacting electrons and holes in semiconductor microcrystals with spherical shape. *Phys. Rev. B* **1988**, *38*, 9797–9805. [CrossRef]
40. Karasiński, P.; Gondek, E.; Drewniak, S.; Kityk, I.V. Nano-sized blue spectral shift in sol–gel derived mesoporous titania films. *J. Sol Gel Sci. Technol.* **2012**, *61*, 355–361. [CrossRef]
41. Tiefenthaler, K.; Briguet, V.; Buser, E.; Horisberger, M.; Lukosz, W. Preparation of planar optical SiO_2-TiO_2 and $LiNbO_3$ waveguides with a dip coating method and embossing technique for fabricating grating couplers and channel waveguides. In *Thin Film Technologies I, Proceedings of the 1983 International Technical Conference/Europe, Geneva, Switzerland, 28 November 1983*; SPIE: Bellingham, WA, USA, 1983; Volume 401, pp. 165–173. [CrossRef]
42. Jiwei, Z.; Xi, Y.; Liangying, Z. Characterization and optical propagation loss of sol-gel derived TiO_2/SiO_2 films. *J. Phys. D Appl. Phys.* **2000**, *33*, 3013–3017. [CrossRef]